THE ROLL OF s AND t UNITARITY IN LHC SOFT SCATTERING AND ITS IMPLICATIONS

Uri Maor

Raymond and Beverly Sackler Faculty of Exact Science

Tel Aviv University, Tel Aviv, 69978, Israel

51st KRAKOW SCHOOL OF THEORETICAL PHYSICS

11-19 JUNE 2011, ZAKOPANE-POLAND

INTRODUCTION

- **Hard QCD deals with the interactions of high transverse momenta partons. These are short distance phenomena which are calculated within the framework of pQCD.**

- **Soft QCD is traditionally associated with low transverse momenta partons separated by large distances. Consequently, we are unable to utilize perturbative methods. The relevant npQCD calculations are, thus, based on phenomenological models, foremost, the Regge pole model.**

- **As we shall see, Pomeron exchange is the leading Regge term. As such, it dominates the soft scattering dynamics at high enough energies. i.e. at and above the CERN $Sp\bar{p}S$ energy.**

In this talk I shall briefly review the original definitions of the Pomeron and its development to its present formulation with special attention to its relevance to LHC physics. The present vigorous studies of the Pomeron and its dynamics are based on sophisticated utilization of ideas dated decades ago:

- S-Matrix Regge Poles, Regge(1957), Chew-Frautchi(1960).
- Reggeon Field Theory, Gribov(1961).
- Eikonal Model, Glauber(1959).
- GW Proton Wave Function Decomposition, Good-Walker(1964).
- Triple Pomeron Formalism, Mueller(1971).
- Multi Pomeron Interactions, Gribov(1968), Kaidalov et al.(1986).
- Pomeron as a 2 gluon color singlet, Low(1975), Nussinov(1976).
- BFKL hard Pomeron, Balitsky-Fadin-Kuraev-Lipatov(1975-1978).

REGGE POLES

Perturbation theory does not apply to soft scattering. We depend, thus, on the phenomenological Regge model which is rooted in S-Matrix theory. A major tool of this approach is to analytically continue a scattering amplitude and its variables from the real axis into the complex plane. This procedure enables us to utilize the powerful methods of complex analysis.

An analytic continuation of the angular momentum into the complex plane was originally suggested by Regge in low energy potential scattering, and was adopted by Chew and Frautchi in their high energy scattering formulation.

Consider an hadronic scattering $a + b \to c + d$, initiated by a t-channel exchange of a spin J meson. Reggeization implies that $J \to Re\,\alpha(t)$. The simplest form of $\alpha(t)$ is linear, $\alpha(t) = \alpha(0) + \alpha' t$. For $t > 0$, $\alpha(t)$ is determined by the measured meson mass spectra. The implication is that a functional description of the meson masses enables a prediction of the scattering dynamics at $t \leq 0$.

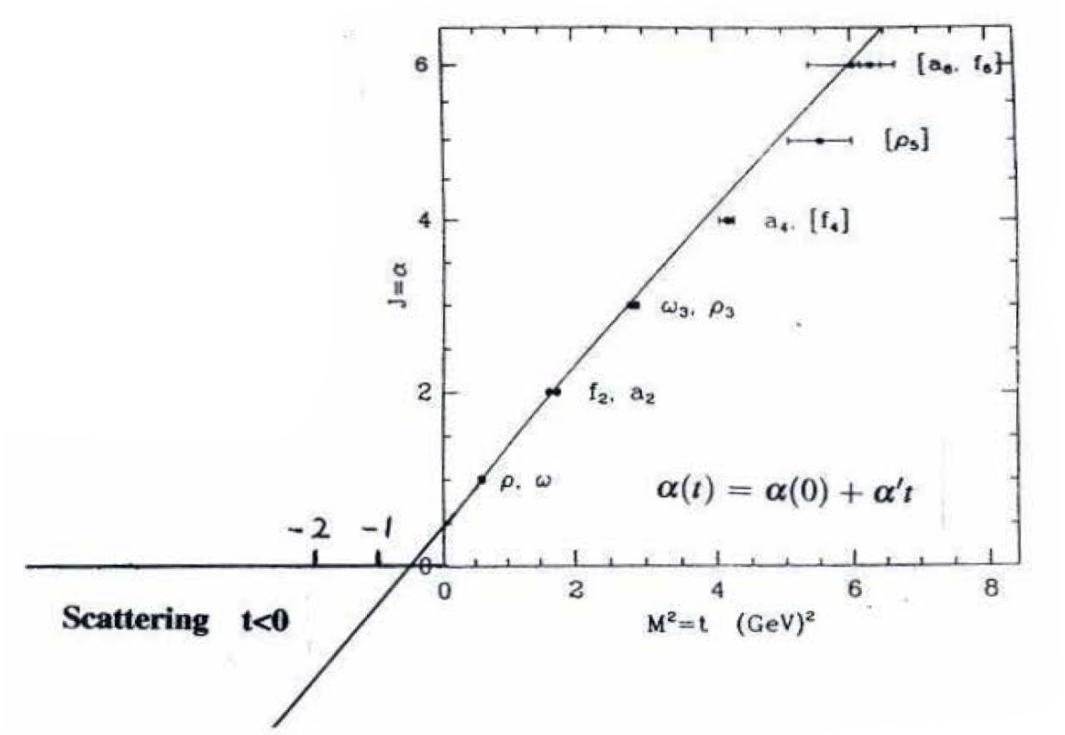

The figure shows the leading meson trajectory with $\alpha(t) = 0.5 + t$. Recall that, for a given trajectory $\sigma_{tot} \propto s^{(\alpha(0)-1)}$ and $\sigma_{el} \propto s^{2(\alpha(0)-1)}$, modulo logarithmic corrections. It leads to a monotonic decrease of $\sigma_{tot} \propto s^{-1/2}$, which is not compatible with the experimental p-p cross sections. The energy dependence of the forward elastic t-slope is controlled by α'.

POMERON MODEL

The original Pomeron, with $\alpha_{I\!P}(0) = 1$, was postulated as an added feature to the Regge model. Theoretically, it is induced by Gribov's Reggeon Calculus. Since the Pomeron trajectory is higher than the Regge contributions, it dominates p-p scattering at high energies.

The total and elastic (but NOT diffractive) cross sections in the ISR-Tevatron range are well reproduced by the simple DL parametrization in which,

$\alpha_{I\!P}(t) = 1 + \Delta_{I\!P} + \alpha'_{I\!P} t$, **where,** $\Delta_{I\!P} = 0.08$ **and** $\alpha'_{I\!P} = 0.25 GeV^{-2}$.

The simple Pomeron model needs considerable re-formulations at high energies, so as to be compatible with s and t unitarity. This goal is executed in impact parameter b-space. Let the elastic scattering amplitude be normalized so that

$$\frac{d\sigma_{el}}{dt} = \pi \mid f_{el}(s,t) \mid^2 \quad \textbf{and} \quad \sigma_{tot} = 4\pi Im f_{el}(s,0).$$

The b-space amplitude is defined $a_{el}(s,b) = \frac{1}{2\pi}\int dq e^{-i\mathbf{q}\cdot\mathbf{b}} f_{el}(s,t)$, $(t = -\mathbf{q}^2)$.

We obtain: $\sigma_{tot} = 2\int d^2b Im a_{el}(s,b)$ **and** $\sigma_{el} = \int d^2b \mid a_{el}(s,b) \mid^2$.

S-CHANNEL UNITARITY

If the Pomeron is super critical ($\Delta_{I\!P} > 0$), σ_{el} grows indefinitely faster than σ_{tot} and will, eventually, get larger! This paradox is eliminated by imposing a unitarity bound on $a_{el}(s,b)$. Enforcing unitarity is model dependent, so I shall start with the simplest diagonal re-scattering matrix, where repeated elastic re-scatterings secure s-channel unitarity: $2Ima_{el}(s,b) = \mid a_{el}(s,b)\mid^2 + G^{in}(s,b)$.

This is no more than a statement that $\sigma_{tot}(s,b) = \sigma_{el}(s,b) + \sigma_{in}(s,b)$.

Its general solution is $a_{el}(s,b) = i\left(1 - e^{-\Omega(s,b)/2}\right)$ **and** $G^{in}(s,b) = 1 - e^{-\Omega(s,b)}$.

$\Omega(s,b)$ **is arbitrary. We obtain a unitarity bound of** $\mid a_{el}(s,b) \mid \leq 2$.

In a Glauber type eikonal approximation the input opacity $\Omega(s,b)$ **is real.**

i.e. $a_{el}(s,b)$ **is imaginary and it equals the imaginary part of the input Born term, a** $I\!P$ **exchange diagram in our context. The output bound is** $\mid a_{el}(s,b) \mid \leq 1$**, which is the black bound. Analyticity and crossing symmetry are restored by dispersion relation (Cauchy theorem) substitution** $s^{\alpha_{I\!P}} \to s^{\alpha_{I\!P}} e^{-\frac{1}{2}i\pi\alpha_{I\!P}}$.

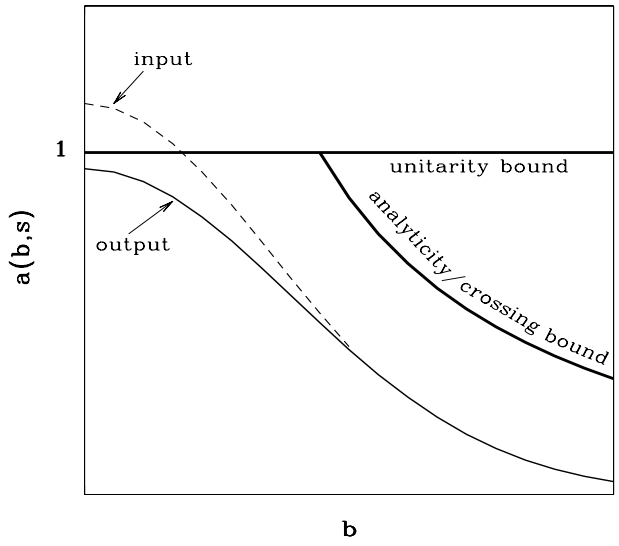

The figure illustrates the effect of eikonal screening restoring s-unitarity.

Total, elastic and inelastic cross sections are:

$$\sigma_{tot} = 2\int d^2b\left(1 - e^{-\Omega(s,b)/2}\right),$$

$$\sigma_{el} = \int d^2b\left(1 - e^{-\Omega(s,b)/2}\right)^2,$$

$$\sigma_{in} = \int d^2b\left(1 - e^{-\Omega(s,b)}\right).$$

Imposing unitarity + analyticity/crossing bounds results in Froissart bound: $\sigma_{tot} \leq Cln^2(s/s_0)$. **This is a numerical (not a functional) bound!**

GOOD-WALKER DECOMPOSITION

Consider a system of two orthonormal states, a hadron Ψ_h and a diffractive state Ψ_D. The GW mechanism stems from the observation that these states do not diagonalize the 2x2 interaction matrix T. Assume that T is diagonalized by Ψ_1 and Ψ_2. We get, $\Psi_h = \alpha\,\Psi_1 + \beta\,\Psi_2, \quad \Psi_D = -\beta\,\Psi_1 + \alpha\,\Psi_2, \quad \alpha^2 + \beta^2 = 1.$

The 4 elastic GW amplitudes are $A_{i,k}^{i',k'} = < \Psi_i\,\Psi_k|\mathbf{T}|\Psi_{i'}\,\Psi_{k'} >= A_{i,k}\,\delta_{i,i'}\,\delta_{k,k'}.$

For initial $p(\bar{p}) - p$ **we have** $A_{1,2} = A_{2,1}$**. The** (i,k) **s-channel unitarity equation is analogous to the one dimensional equation,** $Im\,A_{i,k}\,(s,b) = |A_{i,k}\,(s,b)\,|^2 + G_{i,k}^{in}(s,b).$

$G_{i,k}^{in}$ **is the summed probability for all non GW inelastic processes (including non GW "high mass diffraction") induced by an initial** (i,k) **state.**

As in the one dimensional equation, we have $A_{i,k}(s,b) = i\left(1 - \exp\left(-\frac{\Omega_{i,k}(s,b)}{2}\right)\right),$ $G_{i,k}^{in}(s,b) = 1 - \exp\left(-\Omega_{i,k}(s,b)\right),$ **and** $P_{i,k}^{S}(s,b) = \exp\left(-\Omega_{i,k}(s,b)\right)$**. The** b **space opacities,** $\Omega_{i,k}(s,b)$**, are real, determined by the Born (non screened) input.**

The elastic, SD and DD amplitudes are:

$$a_{el}(s,b) = i\{\alpha^4 A_{1,1} + 2\alpha^2\beta^2 A_{1,2} + \beta^4 A_{2,2}\},$$
$$a_{sd}(s,b) = i\alpha\beta\{-\alpha^2 A_{1,1} + (\alpha^2 - \beta^2)A_{1,2} + \beta^2 A_{2,2}\},$$
$$a_{dd} = i\alpha^2\beta^2\{A_{1,1} - 2A_{1,2} + A_{2,2}\}.$$

Updated eikonal models are multi channel in which:

- $\Omega_{i,k}(s,b) = \nu_{i,k}(s)\,\Gamma_{i,k}(s,b)$.
- **In Regge type models,** $\nu_{i,k}(s) = g_i g_k (\frac{s}{s_0})^{\Delta_{I\!P}}$ **and** $\Gamma_{i,k}(s,b)$ **are parameterized so as to reproduce** $\frac{d\sigma}{dt}$ **of the elastic and diffractive channels in the forward cone.**
- **The eikonal re-scatterings of the incoming projectiles are summed over the GW eigen states.**
- **The net result of the eikonalization procedure is that the input** $\sigma_{tot} \propto s^{\Delta_{I\!P}}$ **and** $\sigma_{el} \propto s^{2\Delta_{I\!P}}$, **behave asymptotically (after screening) like** $ln^2(s)$ **and** $\frac{1}{2}ln^2(s)$.

Induced s-unitarity eikonal screening has a profound effect on the roll played by the various elements which construct the Regge amplitudes.

In the non screened model, $\Delta_{I\!P}$ controls the energy dependence of the scattering amplitude, while $\alpha'_{I\!P}$ controls the t dependence. Recall that, in such a simple model, the total and elastic cross sections, in the ISR-Tevatron range, are well reproduced by DL $\Delta_{I\!P} = 0.08$ and $\alpha'_{I\!P} = 0.25 GeV^{-2}$. The DL parametrization does not apply to the diffractive channels!

The eikonal screening affects the scattering amplitudes s and t dependencies. A higher $\Delta_{I\!P}$ induces stronger screenings affecting the t dependence. It is balanced by a smaller $\alpha'_{I\!P}$. The ISR-Tevatron total and elastic cross sections are well reproduced in a screened model with a large $\Delta_{I\!P}$ and a diminishing $\alpha'_{I\!P}$.

A discussion of the diffractive channels, which are only partially included in the GW mechanism, will be presented coupled to the introduction of multi $I\!P$ interactions.

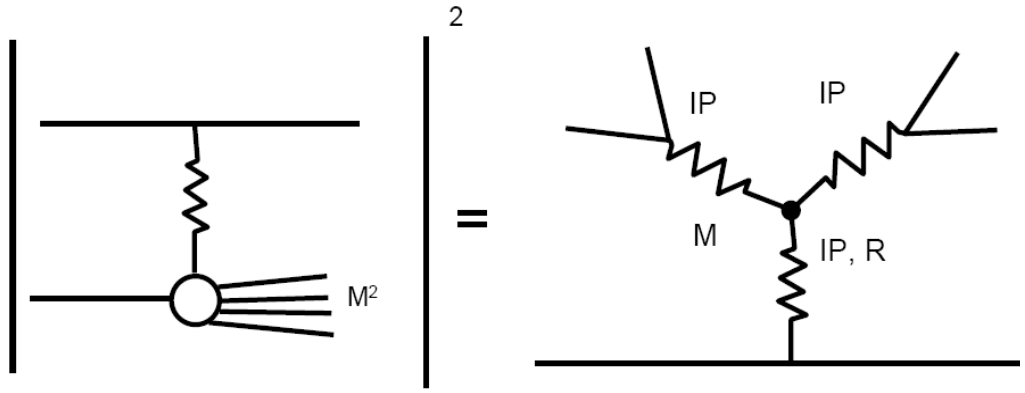

MULTI POMERON INTERACTIONS

Mueller(1971) applied 3 body unitarity to equate the cross section of

$a + b \to M + b$ **to the triple Regge diagram** $a + b + \bar{b} \to a + b + \bar{b}$.

The core of this representation is a triple vertex with a leading $3I\!P$ **term.**

The equation is valid for "high mass diffraction", $\frac{m_p}{M^2} << 1$ **and** $\frac{M^2}{s} << 1$.

The corresponding cross section is $M^2 \frac{d\sigma^{3I\!P}}{dt\, dM^2} = \frac{g_p^2(t) g_p(0) G_{3I\!P}}{16\,\pi^2} \left(\frac{s}{M^2}\right)^{2\alpha_{I\!P}(t)-2} \left(\frac{M^2}{s_0}\right)^{\alpha_{I\!P}(0)-1}$.

$\alpha_{I\!P}$ **connects between** σ_{tot} **and** σ_{el} **s dependencies and** σ_{sd} **high mass dependence.**

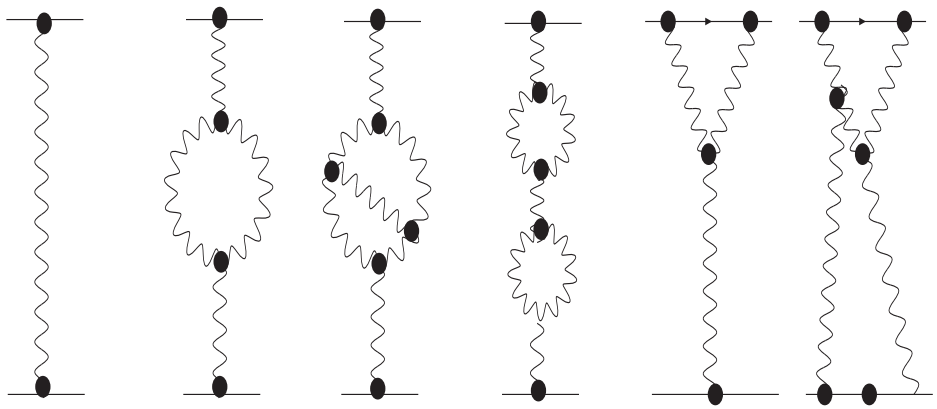

Muller's $3\mathbb{P}$ approximation for "high mass" single diffraction is the lowest order of a very large family of multi Pomeron interactions which are not included in the GW mechanism. This dynamical feature is compatible with t-channel unitarity. The figure shows the low order $\mathbb{P}$ Green's function.

a) Enhanced diagrams which renormalize (in low order) the $\mathbb{P}$ propagator.

b) Semi-enhanced diagrams which renormalize (in low order) the $\mathbb{P}$-p vertexes.

The complexity of these diagrams requires summing algorithms which are model dependent.

Multiple Pomeron interactions initiate additional screening, resulting in a further reduction of the calculated soft cross sections. Note, though, that these features become significant well above the Tevatron energy!

- **The strong screening is a product of the correlated large $\Delta_{I\!P}$ and very small $\alpha'_{I\!P}$ obtained from the adjustment of the $I\!P$ parameters.**
- **The $I\!P$ renormalization diagrams with the adjusted parameters yield a monotonous decrease of $\Delta^{eff}_{I\!P}$ shown in the Table.**
- **A larger value of $\Delta^{input}_{I\!P}$ initiates a stronger reduction of $\Delta^{eff}_{I\!P}$.**

W[TeV]	$1.8 \to 14.0$	$14.0 \to 100.0$
$\Delta^{input}_{I\!P} = 0.335$	0.056	0.041
$\Delta^{input}_{I\!P} = 0.200$	0.078	0.060

LRG SURVIVAL PROBABILITY

An exchanged t-channel Pomeron carries the quantum numbers of the vacuum. This dynamic feature applies to elastic and diffractive scattering.

Its experimental signature is a large rapidity gap (LRG) in the $\eta - \phi$ lego plot devoid of hadrons ($\eta = -ln(tan\frac{\theta}{2})$).

Screening of $I\!P$ exchange reactions are induced by 2 different dynamic processes: s-channel eikonalization and t-channel multi $I\!P$ interactions.

- **GW (elastic+"low mass" diffraction) s-unitarity screening is manifested through eikonalization. It is further being screened by multi $I\!P$ interactions.**
- **Non GW diffraction (soft or hard) screening is expressed by the probability that its LRG signature will not be filled by debris (partons and/or hadrons) originating from either the s-channel re-scatterings of the spectator partons, or by the t-channel multi $I\!P$ interactions.**

- **Denote the gap survival factor initiated by s-channel eikonalization S^2_{eik}, and the one initiated by t-channel multi $I\!P$ interactions S^2_{enh}. $S^2 = S^2_{eik} \cdot S^2_{enh}$.**

In a single channel eikonal model,

$$S^2_{eik} = \frac{\int d^2b \mid M^{in}_{diff}(s,b) \mid^2 P^S(s,b)}{\int d^2b \mid M^{in}_{diff}(s,b) \mid^2}.$$

Recall that, $G^{in} = 1 - P^S$, where, $P^S(s,b) = e^{-\Omega_{I\!P}(s,b)}$. It is the probability that the colliding projectiles reach the $I\!P$ exchange diffractive reaction in their initial state, regardless of their prior re-scatterings.

The calculation of S^2_{eik} in a multi channel model is straight forward, depending on the summation over the GW eigen states. It is:

- **Coherent for an exclusive channel,**

  such as: $p + p \to p + LRG + Higgs(di-jet) + p$.

- **Non coherent for an inclusive channel,**

  such as: $p + p \to X + LRG + Higgs(di-jet) + Y$.

UPDATED POMERON MODELS

Pomeron models have a few components:

- **A bare non screened Pomeron exchange amplitude.**
- **Eikonal re-scatterings of the incoming projectiles secures s-unitarity.**
- **Screening of the elastic and "low mass" diffraction is initiate by the initial re-scatterings.**
- **t-channel unitarity is coupled to multi $I\!P$ interactions, leading to "high mass" diffraction and renormalization of the Pomeron.**
- **Survival probability provides unitarity suppression of non GW diffraction.**
- **Current $I\!P$ models obtain a relatively large $\Delta_{I\!P}$ and a diminishing $\alpha'_{I\!P}$.**
  The value of these parameters have far reaching consequences revealing the theoretical foundations of updated Pomeron models.

Following I shall discuss mainly 3 multi-channel $I\!P$ models in which s and t unitarity screenings are incorporated. The models are very similar conceptually, but differ in their multi $I\!P$ diagram summation procedures and data analyses. I shall, also, refer to 4 single channel eikonal models.

- **GLM(10) (Tel AVIV): has a single soft $I\!P$, $\Delta_{I\!P} = 0.20$, $\alpha'_{I\!P} = 0.02$.**
- **KMR(10) (Durham): $\Delta_{I\!P} = 0.3$, $\alpha'_{I\!P} \propto 1/p_t^2$ is approximated by 3 effective BFKL like trajectories with different $\alpha'_{I\!P}$ values.**
- **Ostapchenko(10) (Bergen): has 2 Pomerons,**

  soft: $\Delta_{I\!P} = 0.17$, $\alpha'_{I\!P} = 0.11$, hard: $\Delta_{I\!P} = 0.31$, $\alpha'_{I\!P} = 0.085$.
- **Kaidalov-Poghosyan(10): is a single channel $I\!P$ model, $\Delta_{I\!P} = 0.12$, $\alpha'_{I\!P} = 0.22$.**
- **Block-Halzen(11), Grau et al.(09), Achilly et al.(11) are single channel eikonal minijet models.**

The Pomeron is defined as a moving Regge pole void of electrical and color charges. The proposition by Low and Nussinov (1975) that the $I\!P$ is a 2 gluon color singlet, is intuitively appealing. This is a Born term description. In high order the 2 gluons are replaced by gluonic ladders.

The microscopic sub structure of the Pomeron is provided in Gribov partonic interpretation of Regge theory, in which the slope of the Pomeron trajectory is related to the mean transverse momentum of the partonic dipoles constructing the Pomeron, $\alpha'_{I\!P} \propto 1/ < p_t >^2$.

The running QCD coupling constant is $\alpha_S \propto \pi/ln\left(< p_t^2 > /\Lambda^2_{QCD}\right) << 1$.

- **GLM utilize the pQCD MPSI procedure, where** $nI\!P \rightarrow mI\!P$ **reduces to a sequence of** $G_{3I\!P}$ **vertexes(Fan diagrams). i.e.** $2I\!P \rightarrow I\!P$ **and** $I\!P \rightarrow 2I\!P$.

- **KMR coupling is** $g^n_m = \frac{1}{2}\, g_N\; nm\, \lambda^{n+m-2} = \frac{1}{2}\, nm\, G_{3I\!P}\, \lambda^{n+m-3}$. $G_{3I\!P} = \lambda g_N$, λ **is a free parameter and** $n + m > 2$. **Kaidalov et al. and Ostapchenko have the same coupling with a different normalization.**

The experimental study of e-p DIS provides a "laboratory" in which we can investigate the Pomeron properties as a function of its kinematic variables.

Indeed, HERA e-p DIS data is a rich source of information on $I\!P$ features.

pQCD study of e-p DIS, in the limit of very high Q^2 and exceedingly small x, led Balitsky, Fadin, Kuraev, Lipatov (1975-78) to introduce the hard BFKL Pomeron corresponding to a hard gluon ladder.

- **The soft $I\!P$ is a simple moving pole in the J-plane,**
  while, the BFKL $I\!P$ is a branch cut.
- **The BFKL $I\!P$ is commonly parameterized as a simple J-pole with $\alpha'_{I\!P} = 0$, which is a signature of the hard $I\!P$.**
- **Recall that in pQCD the BFKL Pomeron slope**
  $\alpha'_{I\!P} \propto 1/Q_s^2 \to 0$ as $s \to \infty$. Q_s^2 is the saturation scale.

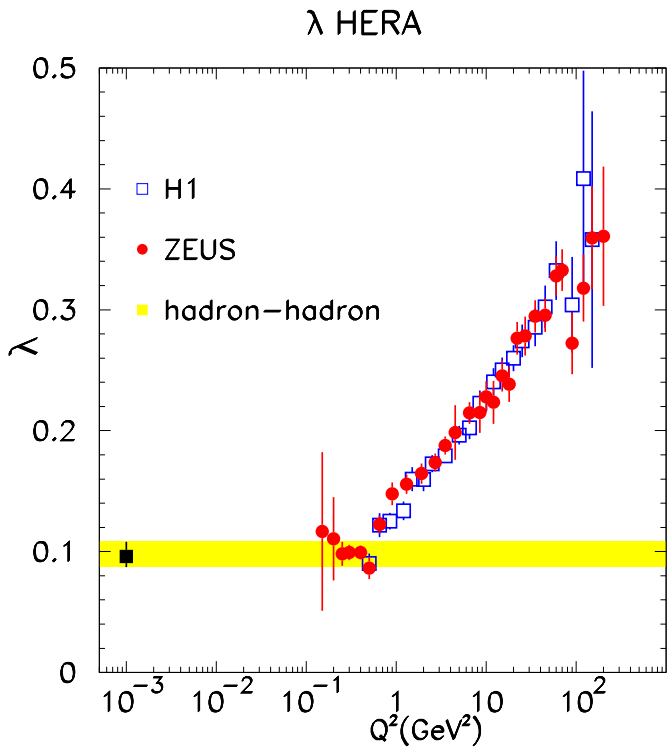

The figure presents $\sigma(\gamma^* + p \to p + X) \propto s^{\lambda}$. $\lambda = \Delta^{eff}_{I\!P}$.

It clearly shows the transition from the soft (non perturbative) Pomeron to the hard (perturbative) Pomeron.

As seen, at very small Q^2, $\Delta^{eff}_{I\!P} \simeq 0.1$, **compatible with the hadronic soft data. At higher** Q^2, **up to** $\simeq 100\, GeV^2$, $\Delta_{I\!P}$ **grows smoothly toward** $\Delta^{eff}_{I\!P} \simeq 0.30 - 0.35$.

To summarize, the basic parameters of the soft and hard Pomerons are:

- **The exact updated soft $I\!P$ parameters are model dependent. In general, $\alpha'_{I\!P}$ is small and $\Delta_{I\!P}$ is large. Given the strong screening induced by these parameters, the effective values of these parameters in the ISR-Tevatron range are compatible with DL.**

- **The parameters of the hard BFKL Pomeron are: $\alpha'_{I\!P} = 0$, reflecting the high p_t of the hard $I\!P$ partons. $\Delta_{I\!P}$ is large, determined by the pQCD calculations.**
  In LO: $\Delta^{BFKL}_{I\!P} = \frac{1}{\pi} 12 \bar{\alpha}_s ln(2) \simeq 0.53$.
  In NLO: $\Delta^{BFKL}_{I\!P} \simeq 0.20 - 0.35$, depending on the renormalization scheme used.

- **As we shall see, the triple $I\!P$ vertex plays an important roll in multi Pomeron interactions. Its value is determined by the data analysis.**

- **The relationship between the soft and hard Pomerons is intriguing and deserves further study.**

DATA ANALYSIS

The essential output of current $I\!P$ models is a a large $\Delta_{I\!P}$ and a very small $\alpha'_{I\!P}$, which initiate s and t screenings. Recall, though, that $\Delta_{I\!P}$ and $\alpha'_{I\!P}$ are just two out of a large number of $I\!P$ model free parameters which have to be adjusted. Current Pomeron models adjust, out of necessity, their free parameters from a small data base. This difficulty was addressed differently by each group.

1) Data Bases:

- **GLM fit a data base having 58 points: $\sigma_{tot}, \sigma_{el}, \sigma_{sd}, \sigma_{dd}$ and B_{el} in the ISR-Tevatron range. We add a consistency check of SD forward slopes and CDF $d\sigma_{el}/dt(t \leq 0.5GeV^2), d\sigma_{sd}/dt\ \ d(M^2/s)(t = 0.05GeV^2)$. The wide energy range of this base necessitates the addition of a secondary Regge contribution.**

- **KMR tune a smaller data base containing just the measured values of $\sigma_{tot}, d\sigma_{el}/dt(t \leq 0.5GeV^2), d\sigma_{sd}/dtd(M^2/s)(t = 0.05GeV^2)$.**

- **Ostapcenko tunes a data base similar to KMR but somewhat larger.**

$\Delta_{I\!P}$	β	$\alpha'_{I\!P}$	g_1	g_2	m_1	m_2
0.2	**0.388**	**0.020** GeV^{-2}	**2.53** GeV^{-1}	**88.4** GeV^{-1}	**2.648** GeV	**1.37** GeV
Δ_R	γ	α'_R	g_1^R	g_2^R	$R^2_{0,1}$	$G_{3I\!P}$
- 0.466	**0.0033**	**0.4** GeV^{-2}	**14.5** GeV^{-1}	**1343** GeV^{-1}	**4.0** GeV^{-2}	**0.0173**GeV^{-1}

2) Adjustment Of The Free Parameters:

The incompatibility between the number of adjusted parameters and size of the data base results with shortcuts and simplifications in the data analysis particular to each group.

- **The data analysis of GLM aims to simultaneously fit the 9 $I\!P$ and 5 Regge parameters. γ is the low energy colorless dipole-target amplitude. We define $\sigma = \frac{1}{2}(\sigma(pp) + \sigma(\bar{p}p))$. Our fitted parameters are displayed in the Table. Our fit has $\chi^2/d.o.f. = 1.56$. A very large contribution to the overall χ^2 stems from 2 SD data points and the CDF value for σ_{tot} at $1800\,GeV$.**

  Neglecting these 3 points we obtain an excellent $\chi^2/d.o.f. = 0.86$.

  Our fit provides a good reproduction of σ_{dd}.

- **KMR and Ostapchenko data bases are predominantly sets of differential cross sections. Such sets have a systemic behaviour and, as such, it is non trivial to obtain a significant "best fit" with a parameter rich model.**

  Both models assume the values of some, less important, parameters.

3) The Approach To The Black Bound:

The basic (post screening) amplitudes are $A_{1,1}$, $A_{1,2}$ and $A_{2,2}$, with which we construct the elastic, SD and DD amplitudes.

$$a_{el}(s,b) = i\{\alpha^4 A_{1,1} + 2\alpha^2\beta^2 A_{1,2} + \beta^4 A_{2,2}\},$$
$$a_{sd}(s,b) = i\alpha\beta\{-\alpha^2 A_{1,1} + (\alpha^2 - \beta^2)A_{1,2} + \beta^2 A_{2,2}\},$$
$$a_{dd} = i\alpha^2\beta^2\{A_{1,1} - 2A_{1,2} + A_{2,2}\}.$$

Recall that, $A_{i,k}$ are bounded by the s-channel unitarity black disc limit.

$a_{el}(s,b)$ reaches this bound at a given (s,b) when, and only when,

$$A_{1,1}(s,b) = A_{1,2}(s,b) = A_{2,2}(s,b) = 1, \quad \textbf{independent of } \beta.$$

Consequently, when $a_{el}(s,b) = 1$, $a_{sd}(s,b) = a_{dd}(s,b) = 0$.

Checking GLM fitted parameters, we note that $g_1 >> g_2$.

Accordingly, the 3 output $A_{i,k}$ amplitudes reach the black bound at different energies. In this case $a_{el}(s, b = 0)$ reaches the black bound when, and only when, the smallest amplitude $A_{2,2}(s, b = 0)$ does.

KMR and Ostapchenko assume that $g_1 = g_2$, which implies that all $A_{i,k}(s, b = 0)$ reach the black bound simultaneously at the same energy.

4) "Low Mass" Versus "High Mass":

- **Good and Walker original study incorporated the few known discrete nuleon isobar states as the diffractive component in their mechanism.**
- **Mueller's triple $I\!P$ approximation is valid when $s >> M^2 >> m_p$. The added "high mass" diffraction is continuous. Its arbitrary high limit is $\frac{M^2}{s} \leq 0.05$.**
- **ISR experimental SD data established the mass continuity above $2.0\,GeV^2$.**

- **Kaidalov, in his breakthrough studies of high energy diffraction, adopted the original GW point of view defining the GW diffracted mass to be small:**
  $Y \leq 3$, corresponding to $M^2 \leq 4.5\, GeV^2$.
  $Y > 3$ defines the non GW "high mass". KMR and Ostapchenko adopt Kaidalov's definitions.

- **GLM offer a radically different approach in which GW diffraction has no Y cut, and it is continuous in M^2 from 2.0 - 0.05s GeV^2. Multi $I\!P$ diagrams generating the non GW diffraction are summed above Y=3.**

- **The net result is that GLM diffraction is predominantly GW, while KMR and Ostapchenko diffraction is predominantly non GW. In the ISR-Tevatron range the difference between the two definitions is small. At LHC energies the difference may be significant.**

	$1.8\,TeV$			$7\,TeV$			$14\,TeV$			$100\,TeV$		
	GLM	**KMR**	**OSTAP**	**GLM**	**KMR**	**OSTAP**	**GLM**	**KMR**	**OSTAP**	**GLM**	**KMR**	**OSTAP**
$\sigma_{tot}\,mb$	**74.4**	**72.8**	**73.0**	**91.3**	**89.0**		**101.0**	**98.3**	**114.0**	**128.0**	**127.1**	
$\sigma_{el}\,mb$	**17.5**	**16.3**	**16.8**	**23.0**	**21.9**		**26.1**	**25.1**	**33.0**	**35.6**	**35.2**	
$\sigma_{sd}\,mb$	**8.9**	**11.4**	**9.6**	**10.2**	**15.4**		**10.8**	**17.6**	**11.0**	**12.7**	**24.7**	
$\sigma_{dd}\,mb$	**4.5**		**3.9**	**6.4**			**6.5**		**4.8**	**7.8**		
S_H^2	**0.11**			**0.06**	**0.024**		**0.04**	**0.015**				

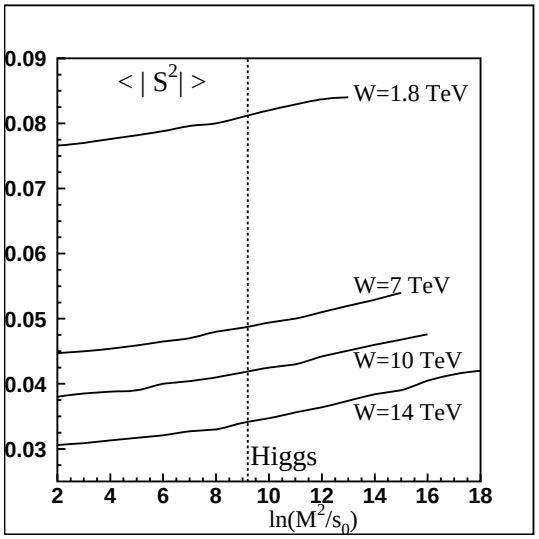

5) Calculated Cross Sections:

The table displays GLM, KMR and Ostapchenko output results.

The figure shows GLM mass dependence of S_H^2. H=Higgs.

- **GLM and KMR total and elastic cross sections are compatible over a remarkable energy range spanning 1.8 to 100 TeV.**
  Ostapchenko is compatible at 1.8. His predictions grow much faster, probably because of the hard $I\!P$ component in his model.
- **GLM and Ostapchenko SD cross sections are compatible. KMR are moderately larger at 1.8 TeV, increasing fast with energy.**
- **KMR refrain from presenting their "high mass" DD cross sections. Their "low mass" DD cross section are negligible over the range of 1.8 to 100 Tev.**
- **Regardless of small differences GLM, KMR and Ostapchenko results at 1.8 TeV are in a reasonable agreement. The main difference between the models is in the formulation and summation procedures of their multi $I\!P$ sector which becomes significant at higher energies.**

LHC Data And Its Interpretation

1)From The Tevatron To LHC:

LHC preliminary data, relevant to this talk, started to become available only recently. The available predictions, regardless of the method with which they were obtained, are based on relatively low energy data analysis.

- **GLM fitted the ISR-Tevatron cross sections, most of them obtained from the ISR.**
- **KMR and Ostapchenko data base is taken from $Sp\bar{p}S$-Tevatron, which is higher in energy but is too limited to support the adjustment of parameter rich models.**
- **The Tevatron data, on its own, does not have the resolution to discriminate between the soft Pomeron models I have discussed.**
  Consequently, a successful reproduction of Tevatron data does not secure a similar success at the LHC.

- **The early LHC cross section data published over the last few weeks can provide the extra resolution needed to discriminate between models and ideas. However, as long as the LHC volume of relevant data will be considerably smaller than the ISR-Tevatron data base, we shall need to apply more sophisticated methods in our data analysis.**

2) Inclusive Pseudorapidity Distributions:

ALICE and CMS have just published the NSD charged multiplicity density $dN_{ch}/d\eta = (1/\sigma_{NSD})d\sigma/d\eta$, **at central pseudorapidity** $-2.5 \leq \eta \leq 2.5$.

This data provides an addional angle to assess the $I\!P$ **models.**

Regretfully, neither KMR nor Ostapchenko have any publications on this topic.

The following is a short summary of the GLM approach.

In the framework of Gribov's $I\!P$ **calculus, single inclusive cross sections can be calculated using Mueller diagrams.**

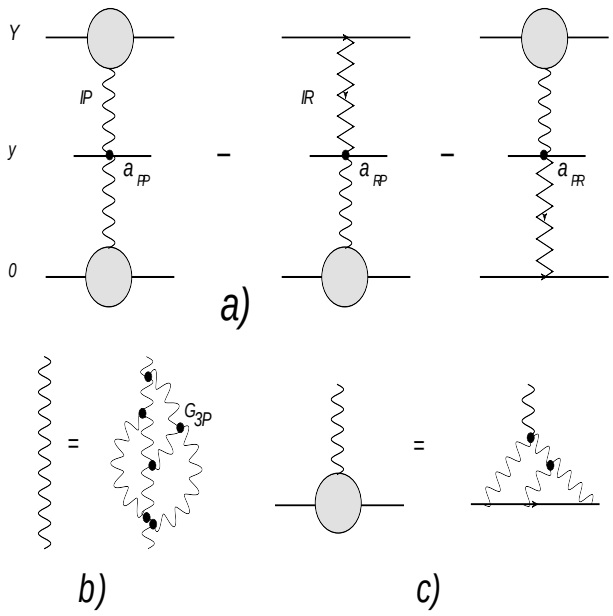

a) Mueller inclusive diagrams, b) $\mathbb{P}$ Green function, c) $\mathbb{P}$-hadron vertex.

A bold waving line = $\mathbb{P}$. A zigzag line = R.

In the calculation, we have used the GLM $\mathbb{P}$ model fitted parameters, to which we have to add 3 additional phenomenological parameters: $a_{\mathbb{P}\mathbb{P}}$ and $a_{\mathbb{P}R} = a_{R\mathbb{P}}$. They account for hadron emission from the $\mathbb{P}$ or Reggeon. Q is the average transverse momentum of the produced minijets with a mass $Q_0 Q$. In BNL minijet studies $Q_0 = 2$ GeV.

Data	$a_{I\!P I\!P}$	$a_{I\!P R}$	Q_0/Q
CMS	0.390	0.186	0.427
All	0.413	0.194	0.356

The inclusive data fit depends, thus, on 3 free parameters. The data base for this fit is obtained from a few experiments spread over many years with different approaches to their error estimates. We have fitted the data twice. Once, fitting the 546, 900, 1800, 2369, 7000 GeV data. The second fitting was confined to the very recent CMS data at 900, 2360, 7000 GeV. The 2 sets of fitted parameters are not identical. The difference between the 2 values of Q/Q_0 is significant for the CMS fits at small η.

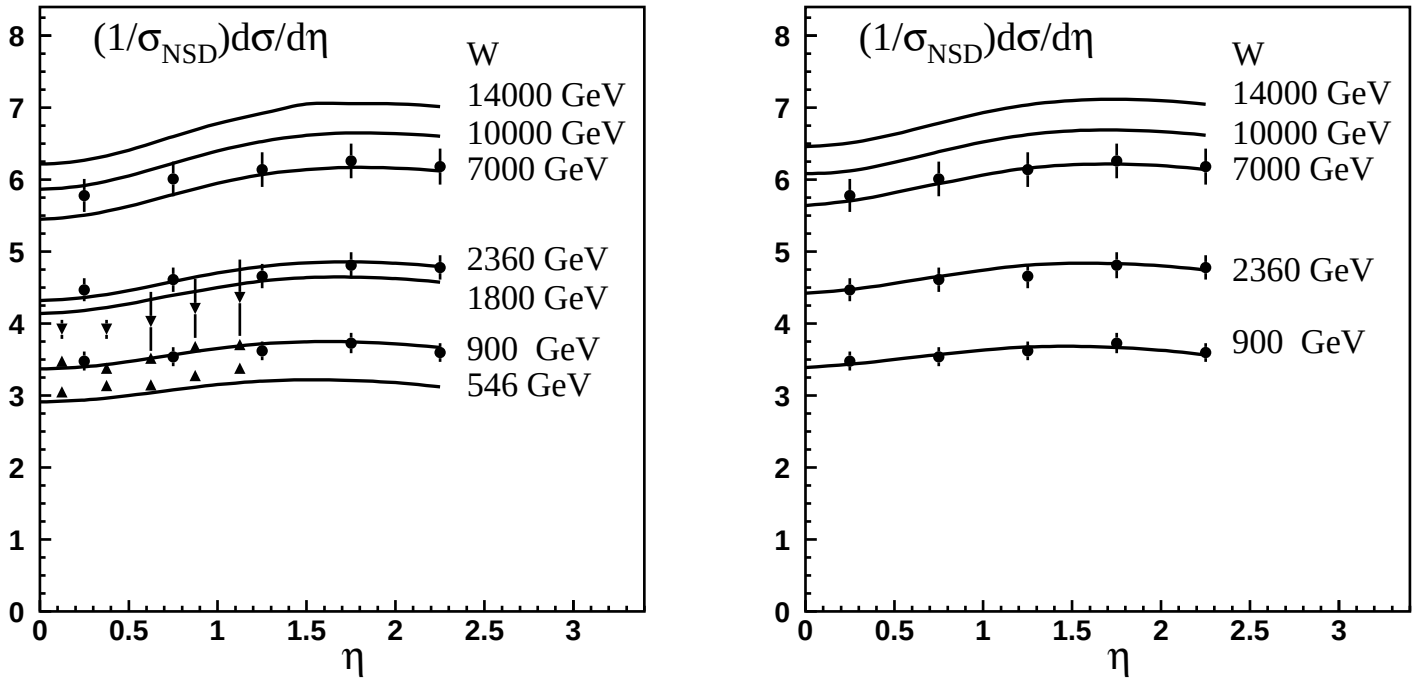

3) Inelastic Cross Sections:

- **The measurement of σ_{inel}, the inelastic cross section, is relatively easy. Indeed, it was measured by ALICE, ATLAS and CMS.**

ATLAS10	ALICE11	Achilli et al.	Block-Halzen	GLM	Kaidalov el al.	KMR
$69.4 \pm 2.4 \pm 6.9$	$72.7 \pm 1.1 \pm 5.1$	60-75	69	68.3	70	62.6-67.1

- **Theoretically, $\sigma_{inel} = \sigma_{tot} - \sigma_{el}$ can be predicted not only by the complicated multi channel unitary models but, also, by single channel models in which the GW mixing is ignored. Recall, though, that single channel models are prone to over estimate the survival probability.**
- **The table compares between the ATLAS10 and ALICE11 measurement at 7 TeV and 5 model predictions.**
- **The energy dependence of σ_{inel} measured by a few collaborations, together with 4 predictions was presented by ALICE 2 weeks ago and will be shown on the next page.**

Comparison with other experiments and models

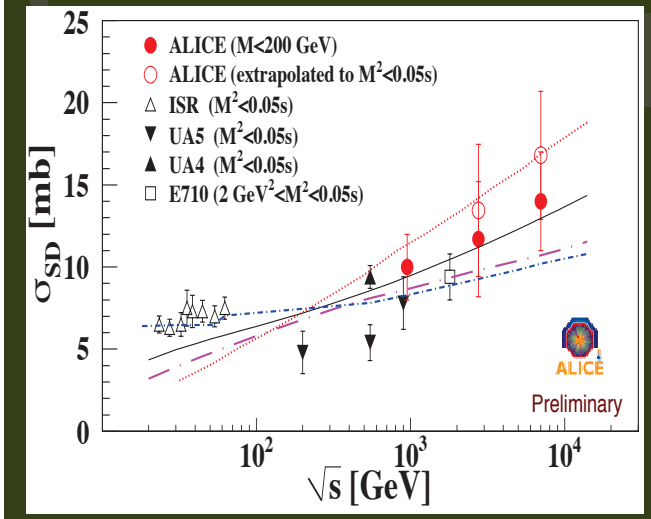

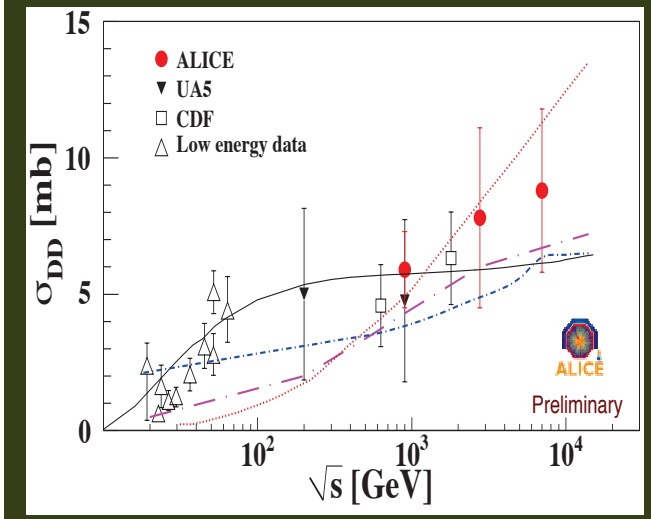

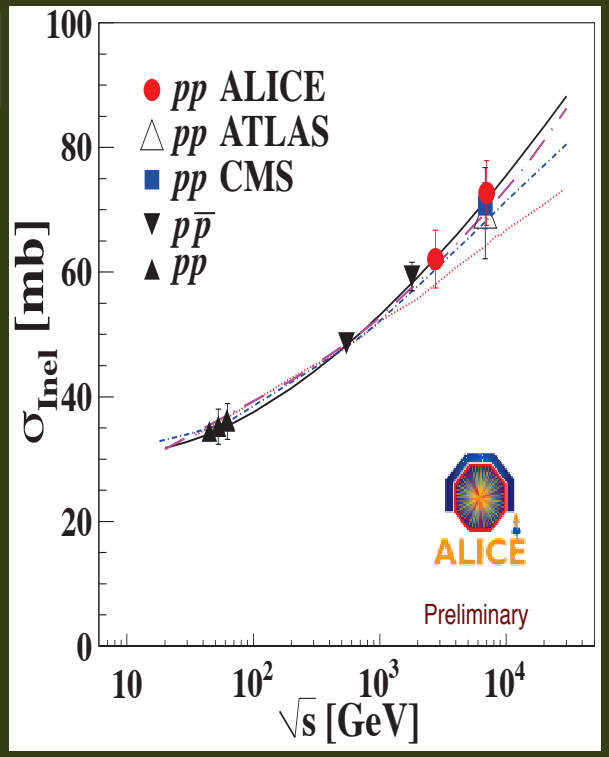

Gotsman et al., arXiv:1010.5323, EPJ. C74, 1553 (2011)

Kaidalov et al., arXiv:0909.5156, EPJ. C67, 397 (2010)

Ostapchenko, arXiv:1010.1869, PR D83 114018 (2011)

Khoze et al., EPJ. C60 249 (2009), C71 1617 (2011)

Model predictions:
SD ➔ $M^2 < 0.05s$
DD ➔ $\Delta\eta > 3$